A&A 417, 1047–1054 (2004)
DOI: 10.1051/0004-6361:20034187

Astronomy & Astrophysics

Doppler imaging of stellar surface structure

XXII. Time-series mapping of the young rapid rotator LQ Hydrae⋆

Zs. Kővári[1,4], K. G. Strassmeier[2,⋆⋆], T. Granzer[2], M. Weber[2,⋆⋆], K. Oláh[1], and J. B. Rice[3]

[1] Konkoly Observatory of the Hungarian Academy of Sciences, 1525 Budapest, Hungary
e-mail: [kovari,olah]@konkoly.hu
[2] Astrophysical Institute Potsdam, An der Sternwarte 16, 14482 Potsdam, Germany
e-mail: [kstrassmeier,mweber,tgranzer]@aip.de
[3] Department of Physics, Brandon University, Brandon, Manitoba R7A 6A9, Canada
e-mail: rice@BrandonU.ca
[4] Collegium Budapest – Institute for Advanced Study, 1014 Budapest, Hungary

Received 12 August 2003 / Accepted 24 December 2003

Abstract. We reconstruct a time series of 28 surface temperature maps (Doppler-images) of the spotted single K2-dwarf LQ Hya from 35 consecutive stellar rotations in Nov.–Dec. 1996. Two more maps are obtained from data in late April and early May 2000. All maps show spot activity preferably at low latitudes between −20° and +50°, with a concentration in a band centered at around +30°, and with only occasional evidence for a higher-latitude spot extension. No trace of a polar spot is found at any of the above epochs. Most of this morphology can be reproduced by our flux-tube emergence model, except for the equatorial activity where the strong Coriolis force due to the rapid rotation always deflects flux tubes to higher latitudes. We also present the detection of weak differential surface rotation from a number of cross-correlation maps of the time-series images in late 1996. A solar-type differential rotation law, i.e. the equator rotating faster than the poles, with $\Delta\Omega = +0.022$ rad/day (lap time of ≈280 days) is in agreement with the data. Using the available photoelectric observations from 21 years we refine the rotation period to 1.60066 ± 0.00013 days and find a remarkable phase coherence over the course of 21 years, supporting the recent finding of active longitudes by Berdyugina et al. Furthermore, our photometry shows a complex multi-cyclic long-term brightness variability with three periods of 13.8 ± 2.8 years, its harmonic 6.9 ± 0.8 and 3.7 ± 0.3 years, respectively. The 3.7-year period would be in good agreement with the fundamental-mode oscillation period predicted by Kitchatinov et al. from a distributed-dynamo model, but remains to be confirmed.

Key words. stars: activity – stars: imaging – stars: individual: LQ Hydrae – stars: late-type – stars: starspots

1. Introduction

LQ Hydrae was first recognized by Bidelman (1981) and Heintz (1981) due to its strong Ca II H&K emission. In an early paper by Eggen (1984) it was noted as a candidate star with a "very active chromosphere". Fekel et al. (1986a) detected Hα as an absorption line filled-in by chromospheric emission and suggested that LQ Hya is a spotted BY Dra-type variable. They also derived a $v \sin i$ of 25 km s^{-1}, thus verified it to be a rapid rotator. Later on, Fekel et al. (1986b) found its radial velocity to be constant and in agreement with the overall motion of the Pleiades cluster and determined a photometric period of 1.6603 days, which was interpreted as the rotation period of this single spotted star. Coronal activity was subsequently detected by its strong 6-cm radio emission flux of 0.25 ± 0.06 mJy (Drake et al. 1990) and by the ROSAT all-sky survey at soft X-ray wavelengths. From the latter detection, Sterzik & Schmitt (1997) determined a (logarithmic) normalized luminosity of $\log L_X/L_{bol}$ of −3.06, which makes LQ Hya one of the most active stars of its mass and puts it in the so-called saturation domain. Later, strong flares were detected with ROSAT and ASCA by Covino et al. (2001) and in the ultraviolet and optical range by Montes et al. (1999).

On the basis of the Li abundance and space motions, Fekel et al. (1986b) concluded that LQ Hya is on or near the zero-age main sequence and still maintaining most of its rotational momentum but is a field star. It is thus a good example of a violently active young Sun despite its somewhat lower mass. Observations of LQ Hya could link the dynamo behavior of

Send offprint requests to: K. G. Strassmeier,
e-mail: kstrassmeier@aip.de

⋆ Table 1 and Fig. 5 are only available in electronic form at http://www.edpsciences.org

⋆⋆ Visiting Astronomer, National Solar Observatory, operated by the Association of Universities for Research in Astronomy, Inc. under contract with the National Science Foundation

the weak-lined pre-main-sequence stars to that of young main-sequence stars. This spurred considerable interest in the community and many papers followed.

Rapid spot evolution was reported on timescales from a few weeks to months (Jetsu 1990, 1993; Strassmeier et al. 1997, 1999), while the total spot coverage hinted towards a cyclic behavior with a 6–7 year-long period.

The first Doppler image from the star was produced by Strassmeier et al. (1993) for the epoch 1991.08. In Paper VII (Rice & Strassmeier 1998) we compared Doppler images of LQ Hya from lines with a large range of equivalent widths, including previously published maps from Saar et al. (1994). The polar feature that we saw in the average March 1995 map was not evident from the comparably strong Ca I 6439 and Fe I-6430 line reconstructions but rather due to several weaker Fe and Ni lines near 6170 Å. The "polar" feature in these maps was dominated by its coolest part, which appeared off-centered with respect to the pole at a latitude of +70°. Berdyugina et al. (2001) preliminary maps from January, May, and October 1995 from the same spectral region near 6170 Å did not show a polar spot at all but just a single high-latitude feature centered at a latitude of +60°. The average temperature contrast of the spots in their images was 900 K, in agreement with our values of between 800–1200 K. An independent map from data taken within our time slot is the "spot-occupancy" image by Donati (1999) from 1996.99. It consists of a number of low-latitude features between 0°–40° in principle agreement with our 1996/E map. Donati's image showed additionally a small but apparently significant polar feature.

In the present paper, we apply the Doppler imaging technique to, firstly, a data set of 35 spectra obtained within two months in late 1996 and, secondly, to two further data sets in late April and early May 2000, separated by approximately two weeks. The data will be described in Sect. 2. Section 3 summarizes our analysis of the photometric variability and Sect. 4 deals with the Doppler-imaging analysis. The results are discussed in Sect. 5.

2. Observations

2.1. Spectroscopy

The bulk of our spectroscopic data were collected at the National Solar Observatory (NSO) with the 1.5 m McMath-Pierce telescope during 57 consecutive nights in November–December 1996. Two further observing runs were granted at Kitt Peak National Observatory (KPNO) with the 0.9 m coudé-feed telescope in late April and early May 2000, just two weeks apart.

At NSO, we used the stellar spectrograph with Milton & Roy Grating 1 and the 105 mm transfer lens that resulted in a resolving power of 42 000. A resolution element consisted of 1.6 pixels. All observations utilized the 800 × 800-pixel TI CCD with a dispersion scale of 0.10 Å/pixel. The integrations on LQ Hya have a typical signal-to-noise (S/N) ratio of about 150–200:1 in the continuum and were made in a 50-Å wide wavelength region centered at 6440 Å. The observing log and radial velocities are presented in Table 1 (available on-line at EDP Sciences). The five colums of the table list the HJDs and phases of the spectra, the radial velocity measurements with their errors and the corresponding image numbers as used in Sect. 4 of this paper.

The new KPNO data from April 2000 were obtained with the coudé-feed telescope and the coudé spectrograph equipped with grating A, camera 5, the long collimator and the 3096 × 1024 CCD (F3KB chip, 15 μpixels). The spectra covered 300 Å and were centered at 6500 Å. The effective resolution with the F3KB CCD was just 27 000 (11 km s^{-1}) as compared to 42 000 (7 km s^{-1}) with the NSO stellar spectrograph. With the former, we achieved signal-to-noise ratios of about 250:1 in 45-min integration time.

Data reductions were carried out in the standard fashion with the NOAO/IRAF software package and included the standard tasks of bias subtraction, flat fielding, (optimal) aperture extraction, and cosmic-ray clipping.

2.2. Photometry

The new photometric data in this paper was obtained with the Amadeus 0.75-m automatic photoelectric telescope (APT), part of the University of Vienna twin APT at Washington Camp in southern Arizona (Strassmeier et al. 1997), and the 0.25-m Phoenix APT located at the same site (Seeds 1995). The Amadeus photometer was equipped with Johnson-Cousins VI filters, while the Phoenix APT was used with Johnson UBV. All observations were made differentially with respect to HD 82447 as the comparison star ($V = 6\overset{\mathrm{m}}{.}125$, $V-R_C = 0\overset{\mathrm{m}}{.}618$, $V-I_C = 1\overset{\mathrm{m}}{.}18$) and HD 82508 as the check star. The new data cover the time interval 1996 through 2003. All photometry was transformed to match the Johnson-Cousins $UBV(RI)_C$ system.

Altogether, we add 987/1089/1077 $U/B/V$ data points from the Phoenix APT and 621/621 V/I_C data points from the Amadeus APT.

3. The quest for the correct rotation period

Our photometric data base densely covers 21 years, starting with the discovery of the light variability in late 1982 (Fekel et al. 1986b) until close to the submission date of this paper. Altogether we use 4891 V-band data points, each with a precision better than 1%, many of them even better than 0.5% (see, e.g., Strassmeier et al. 1997). The period analysis is performed with MUFRAN (Kolláth 1990). However, the input data is not the original observations as for the cycle search but the pre-whitened data with the long-term trend and the cycle period removed (Fig. 1, top left panel).

The top right panel of Fig. 1 shows the periodogram from the pre-whitened V data. The largest peak corresponds to a period of 1.60066 ± 0.00013 days. A straightforward comparison with the period obtained from the original data, i.e. the original measurements not pre-whitened, shows a difference of 5×10^{-6} days, i.e. roughly two orders smaller than the anticipated error. The error is computed from the width of the frequency peak according to the prescription in Bevington (1969) but we note that nightly and seasonal instrumental and

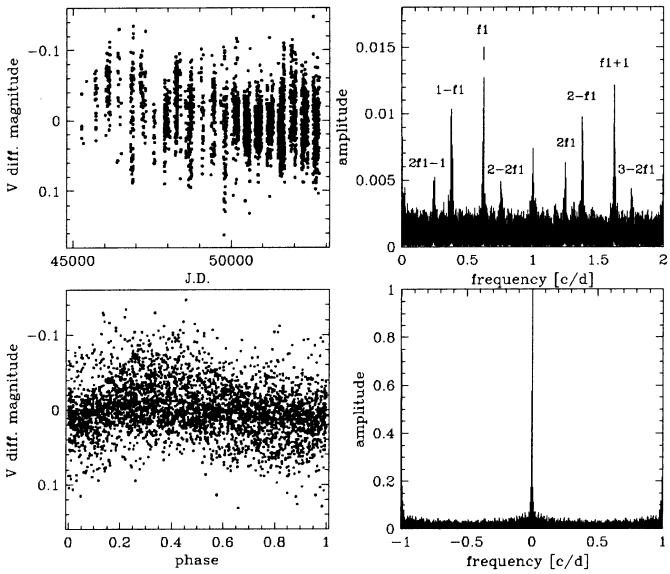

Fig. 1. The rotational-modulation signature from the long-term V data. *Top left*: input V data for the frequency analysis after pre-whitening with the long-term trend and the 3.7-year period. *Top right*: its frequency spectrum. f_1 is the true photometric period of 1.60066 days, also marked are several of its aliases. *Bottom left*: phase plot of 21 years of V data with f_1. The continuous line is a simple sine-curve fit. *Bottom right*: spectral window of the frequency analysis.

extinction variations set a practical limit to the application of this criterion.

The period of 1.60114 days obtained by Jetsu (1993), and used in the recent study by Berdyugina et al. (2002), has a time base of less than half of the data in the present paper and has much less data points. For the first ten years of our dataset (which is nearly identical with Jetsu's) we get $P_{\rm rot}$ = 1.6011 ± 0.0002, whereas the second eleven years alone result in $P_{\rm rot}$ = 1.6007 ± 0.0003. The rotational period is found from the spotted light curves, that are subject to phase discontinuities because of the newly emerging spots at different longitudes. The longer time-base allows us to derive a more precise period, which is, thus, not necessarily the average of the periods found from different data subsets. We also note that our new period achieves a very high degree of phase coherence over the 21 years of data (Fig. 1, lower left panel). The residual light curve exhibits a preferred minimum brightness at phase $\approx 0\overset{\rm p}{.}9$ and a preferred maximum brightness at phase $\approx 0\overset{\rm p}{.}4$, i.e. 180° apart, and thus supports the finding of active longitudes by Berdyugina et al. (2002), despite that we arrived at a significantly different rotational period for LQ Hya.

We remind the reader that even small differences of the rotational period can be critical for the phasing of *long-term* spectroscopic data but is uncritical for combining phased data from short periods of time, say, a month. Therefore, a new ephemeris of

$$\mathrm{HJD} = 2\,448\,270.0 + (1.60066 \pm 0.00013) \times E, \qquad (1)$$

is derived, where the zero point is an arbitrary point in time, as was used for our previous Doppler images in 1991 and 1995.

Table 2. Astrophysical data for LQ Hya.

Parameter	Value
Classification	K2V
Distance (Hipparcos)	18.35 ± 0.35 pc
Luminosity, L	0.270 ± 0.009 $L_\odot$
$\log g$	4.0 ± 0.5
$T_{\rm eff}$	5070 ± 100 K
$(B-V)_{\rm Hipparcos}$	0.933 ± 0.021 mag
$(V-I)_{\rm Hipparcos}$	1.04 ± 0.02 mag
$v \sin i$	28.0 ± 1.0 km s^{-1}
Inclination, i	65° ± 10°
Rotation period, $P_{\rm rot}$	1.60066 ± 0.00013 days
Radius, R	0.97 ± 0.07 $R_\odot$
Microturbulence, ξ	0.5 km s^{-1} (adopted)
Macroturbulence, $\zeta_{\rm R} = \zeta_{\rm T}$	1.5 km s^{-1} (adopted)
Chemical abundances	solar ±0.1 dex
Age	≈100 Myr
Mass	≈0.8 $M_\odot$

4. Doppler images

4.1. Astrophysical data for LQ Hya

Astrophysical input parameters for LQ Hya are collected in Table 2. We adopted $V = 7\overset{\rm m}{.}75 \pm 0\overset{\rm m}{.}02$ and $B = 8\overset{\rm m}{.}64 \pm 0\overset{\rm m}{.}02$ as the unspotted magnitudes. These values were the brightest magnitudes observed so far in 1993/94 and likely represent the existence of an unspotted hemisphere, at least to first order. The absolute visual magnitude based on the Hipparcos parallax (ESA 1997) is then $+6\overset{\rm m}{.}43 \pm 0\overset{\rm m}{.}04$ and, with above unspotted $B-V$ of $0\overset{\rm m}{.}89$ and its corresponding effective temperature of 5070 K and bolometric correction of −0.277 from the calibration of Flower (1996), the luminosity of LQ Hya is 0.270±0.009 $L_\odot$ (adopting $+4\overset{\rm m}{.}73$ as the Sun's bolometric magnitude and no errors for $T_{\rm eff}$).

We adopt an inclination of 65°, taken from our Paper VII (Rice & Strassmeier 1998). Note that potential errors of ±10° in the inclination have only very minor impact on the maps.

Our best value for $v \sin i$ of 28±1 km s^{-1} (see also Paper VII, and the discussion in Donati 1999) combined with $P_{\rm rot}$ = $1\overset{\rm d}{.}60066$ yields $R \sin i = 0.88 \pm 0.03\ R_\odot$. An average K2 dwarf is expected to have a radius of ≈0.75 $R_\odot$, significantly smaller than the minimum value from $v \sin i$ and $P_{\rm rot}$. Because we can exclude a $v \sin i$ error of 6–7 km s^{-1}, which would be needed to bring the minimum radius in agreement with the expected value given that $i \approx 65°$, we interpret the larger than normal radius as evidence that LQ Hya is still a ZAMS star. Its rapid rotation and moderately-high lithium abundance is in good agreement with this interpretation.

In Fig. 2, we compare theoretical pre-main sequence evolutionary tracks for 0.7, 0.8, and 0.9-$M_\odot$ stars with the observed position of LQ Hya. While D'Antona & Mazzitelli (1997) use the – essentially parameter-free – Full Spectrum of Turbulence (FST) model to treat convection, the other models are based on Mixing Length Theory (MLT). Granzer et al. (2000) use a mixing-length parameter of α = 1.67 to tune a 1 $M_\odot$ star at 4.85 Gyr to our present Sun, Chabrier & Baraffe (1997)

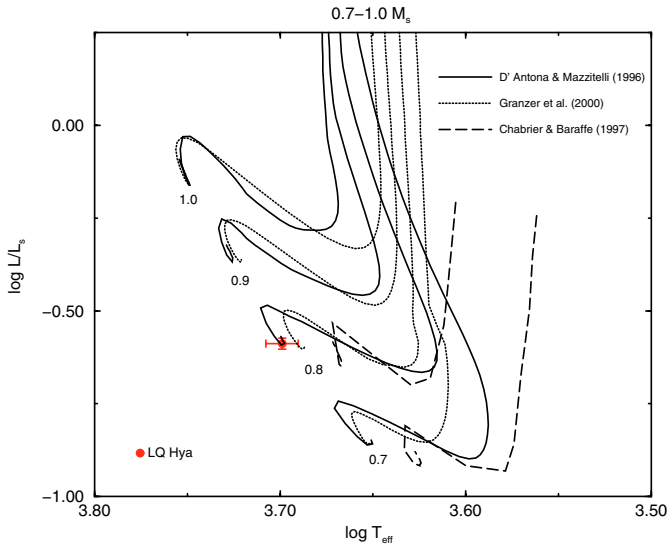

Fig. 2. The position of LQ Hya in the HR-diagram compared to three different pre-main-sequence tracks for masses of 0.7, 0.8 and 0.9 $M_\odot$. The solid lines are tracks from D'Antona & Mazitelli (1997), the dotted lines are tracks from Granzer et al. (2000), the dashed lines are tracks from Chabrier & Baraffe (1997) – see text. Superimposed is the position of LQ Hya, based on the Hipparcos distance and our new photometry as well as spectroscopy. The position of LQ Hya is in agreement with a 0.8 $M_\odot$ star at an age of roughly 100 Myrs.

use $\alpha = 1.00$ for all of their models. The observed properties of LQ Hya agree with the 0.8-$M_\odot$ ZAMS position from the D'Antona & Mazzitelli tracks. However, this does not imply that we can conclude that the D'Antona & Mazzitelli tracks, and thus also FST convection, are superior to the other models. Some authors claim (e.g. Baraffe et al. 1997) that the D'Antona & Mazzitelli tracks generally tend to lie at too high a $T_{\rm eff}$. Nevertheless, the position of LQ Hya in the HR-diagram suggests it to be a ≈0.8-$M_\odot$ star at an age of roughly 100 Myrs, in agreement with previous estimates of "Pleiades-age".

4.2. The TempMap line-profile inversion code

Our line-profile inversion code performs a full LTE spectrum synthesis by solving the equation of transfer through a set of Kurucz (1993) model atmospheres, at all aspect angles, and for a given set of chemical abundances. Simultaneous inversions of up to eight spectral lines, as well as two photometric bandpasses, are then carried out using a maximum-entropy regularization. The adopted atomic line parameters are identical to the ones listed in previous papers in this series. We assumed solar abundances for all elements, but for fine tuning we altered the transition probabilities ($\log gf$'s) of some – mostly V I – blends to obtain a better fit to the spectra. We note here that the effect on the reconstruction when changing $\log gf$ of a given line (within a reasonable range) is not distinguishable from changing its elemental abundance. A more detailed description of the TempMap code and additional references regarding the inversion technique can be found in Rice et al. (1989), Piskunov & Rice (1993), Rice & Strassmeier (2000) and most recently in Rice (2002).

4.3. Phase-combined Doppler images for late 1996

The spectra from winter 1996 were divided into five data subsets, "1996/A" "B", "C", "D" and "E". The corresponding mean JDs are (2 400 000+) 50 400.520, 50 415.647, 50 426.012, 50 435.416 and 50 446.265, merging 8.0, 7.4, 5.0, 4.4, and 6.2 stellar rotations, respectively. The Doppler-maps and the line-profile and light-curve fits are shown in Fig. 3 along with an image from all data combined. The small light and color amplitudes of $\Delta V \approx 0\overset{\rm m}{.}06$ and $\Delta(V-I) \approx 0\overset{\rm m}{.}01$ already suggested a fairly homogeneous low-contrast surface spot distribution. The Doppler images actually show spots mostly within a band at low to mid latitudes between, say, −20° to +50°, in agreement with our previous results in Paper VII.

There is also reasonable well agreement between maps from different spectral lines despite that the Ca I line at 6439 Å provides less detailed and less contrasted maps relative to the Fe I-6430 line. Accordingly, the average temperature contrast of the coolest regions with respect to the unspotted photosphere of ≈5200 K is different for the two lines, i.e. 1000 ± 120(rms) K from the Fe maps, and 800 ± 100(rms) K from the Ca map, respectively. This error is comparably independent of the type of inversion algorithm once a certain S/N of the observations is encompassed, and is then dominated by external errors in the spectra and the atomic and atmospheric data. For our LQ Hya spectra, we estimate $\Delta T \pm 200$ K per surface resolution element based on our numerical simulations (Rice & Strassmeier 2000).

Each of the five subsets combine spectra from between 4–8 stellar rotations. Therefore, shorter-lived features than this, if existent, may be seen only in one or a few line profiles per map, and any attempt by the program to fit these profiles will not succeed unless it adds spurious features at some other places to find an even smaller sum of the residuals squared. In general, the code is very robust against such non-periodic features and simply refuses to fit a particular bump in the line profile, but some additional uncertainty will be introduced.

4.4. Phase-combined Doppler images for 2000

The year-2000 data were taken during two observing runs, "2000/A" and "2000/B", with approximately two weeks in between. These subsets cover ≈3 and ≈5 consecutive stellar rotations, respectively, and the corresponding mean JDs are (2 400 000+) 51 641.863 and 51 664.915. The resulting maps for three spectral regions are shown in Fig. 4. The recovered spot distributions are very similar to the ones obtained in 1996, i.e. spots are predominantly located at low-to-mid latitudes possibly including the stellar equator. Again, there is good agreement between the main features on the respective Fe and Ca images. Both Fe lines suggest ≈200-K cooler features as in 1996, i.e. ≈1200 ± 120(rms) K, while the spots from the Ca profiles come out 100-K warmer than in 1996, i.e. ≈900 ± 100(rms) K. However, with an estimated external error of 100–200 K per surface resolution element, this difference is not significant and most likely not real.

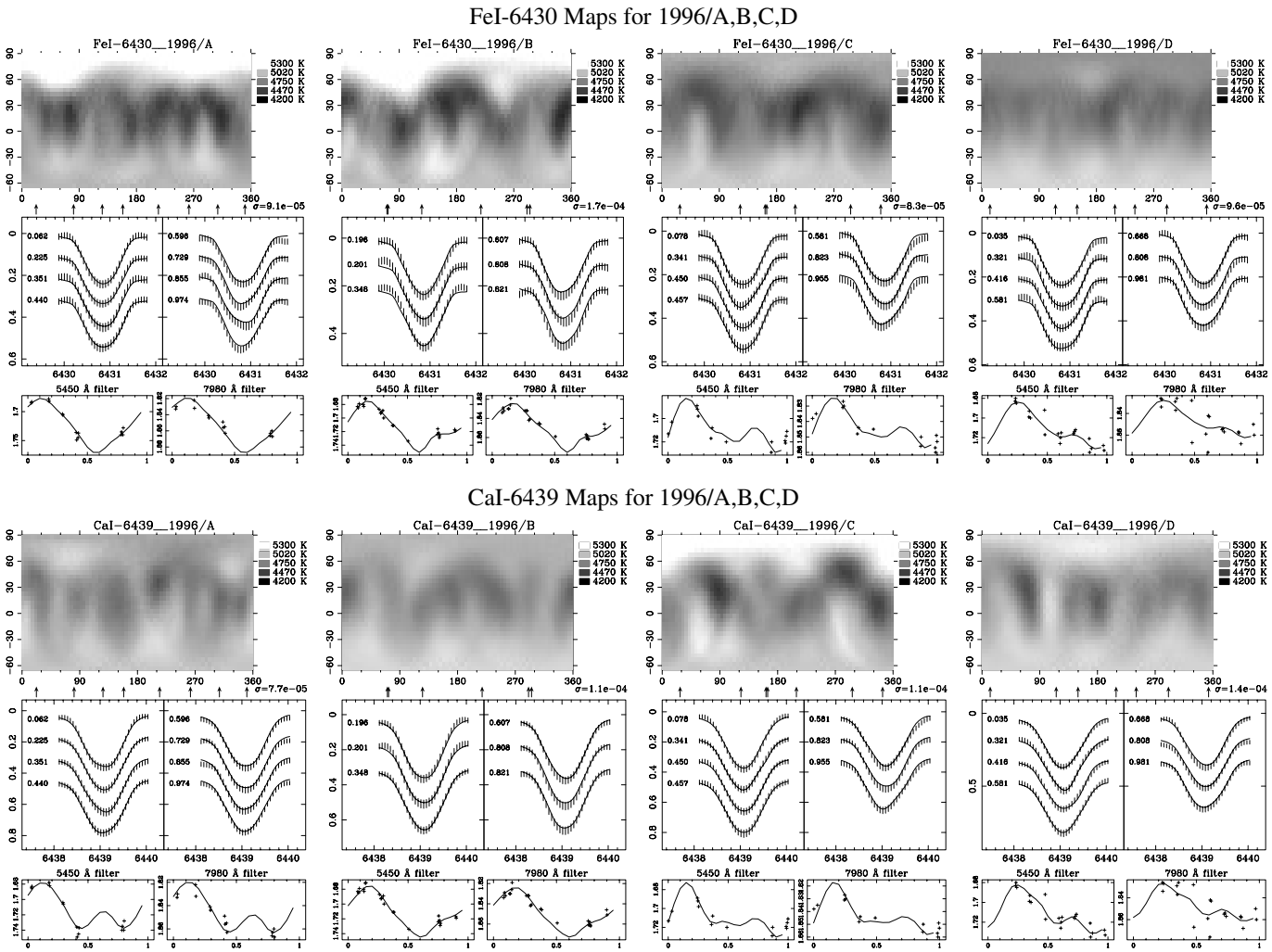

Fig. 3. Rotationally-phased maps for Nov.–Dec. 1996 (subsets "A", "B", "C", "D" and "E", and the entire data set "A–E"). The top part of the figure shows the results from Fe I 6430-Å line and the lower part from the Ca I 6439-Å line. The maps are presented in a pseudo-Mercator projection from latitude −65° to +90°. The line profiles and their fits are shown in the respective middle rows, the light curves and their fits are plotted in the bottom rows for the Strömgren *b* and *y* bands, respectively. The phases of the observations are marked by arrows below the maps and the overall goodness of fit, σ, is indicated just to its right.

4.5. Time-series Doppler images

From the 35 spectra taken during the 1996 observing run (covering 35 consecutive stellar rotations), we built 28 data subsets with eight spectra each (a total of three spectra with low S/N due to clouds was discharged). The first subset consists of the first eight observations listed in Table 1, i.e. is identical to our subset "1996/A" from Sect. 4.3. The next subset is formed from omitting the first spectrum from the beginning and adding the subsequent one to the end. This pattern is continued until the last eight spectra are included (for an earlier application of this method see also Strassmeier & Bartus 2000, Paper XII of this series). The result is a time series of altogether 28 images which may reveal information on short-term spot changes. Fig. 5 (available on-line only) shows the time series for the Fe I-6430 line (the Ca maps, as well as a short movie for both lines, can be viewed on our research home page at `www.aip.de`).

5. Discussion and conclusions

5.1. Multiperiodicity in the brightness of LQ Hya

A detailed Fourier-analysis revealed a quasi-periodic cycle of the brightness that is best fit with a combination of a period of 13.8 ± 2.8 years and its first harmonic 6.9 ± 0.8 years. Prewhitening the dataset with these periods, we possibly see another cycle with 3.7 ± 0.3 yrs. We note that our new value is still very close to the (3σ) noise limit and remains to be confirmed (cf. Oláh & Strassmeier 2002). Periods of 15 and 7.7 years were confirmed by a similar study by Berdyugina et al. (2002). This "cycle" has not repeated yet, and thus any interpretation is premature. Besides this long-term trend the data also hint towards a shorter period with a length of 3.7 years. This period would be in good agreement with the fundamental-mode oscillation period of 3.2 years predicted by Kitchatinov et al. (2000) from a distributed-dynamo model applied to LQ Hya. Unfortunately,

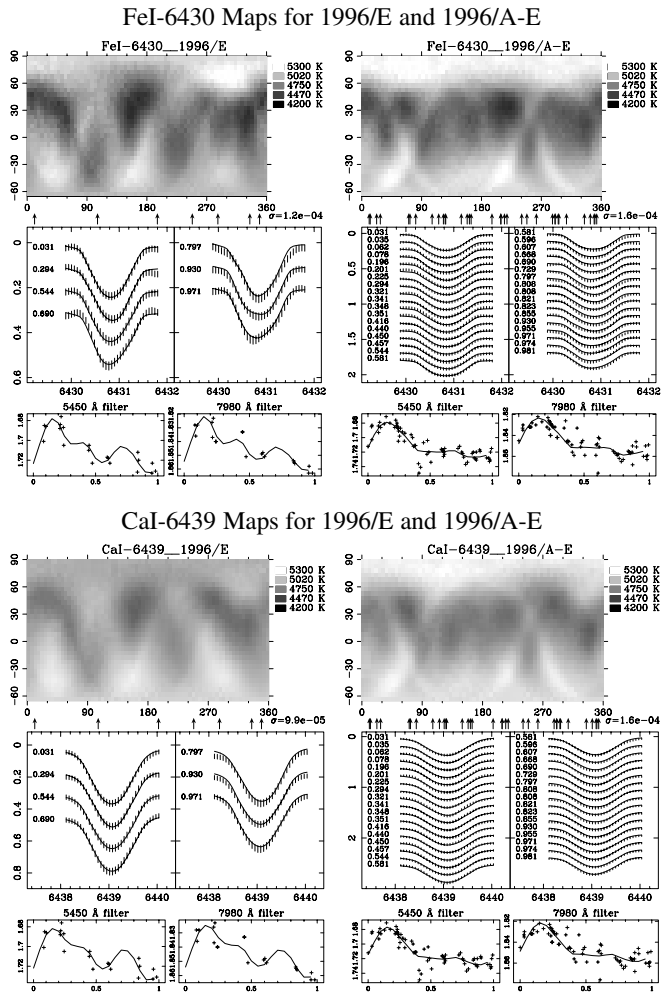

Fig. 3. continued.

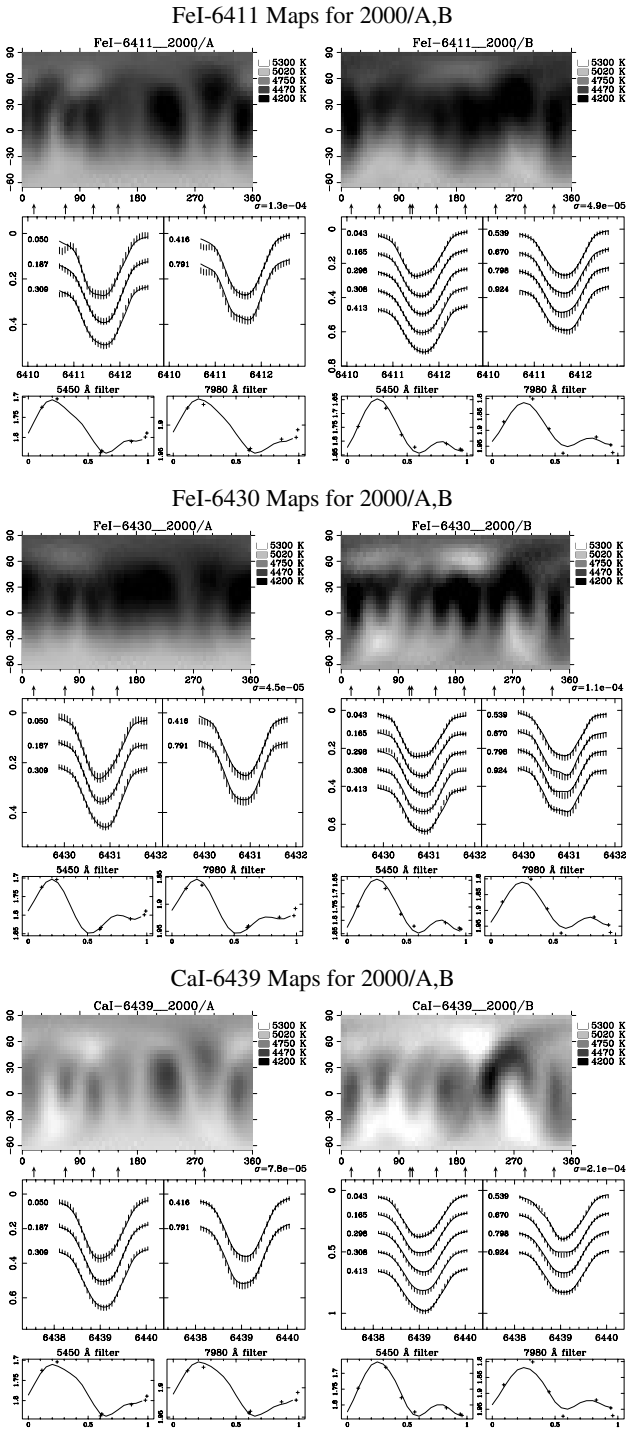

Fig. 4. Rotationally-phased maps for April and May 2000. *From top to bottom*: Fe I 6411-Å, Fe I 6430-Å and Ca I 6439-Å images for the subsets "A" (April) and "B" (May), respectively. The maps are presented in a pseudo-Mercator projection as in Fig. 3.

the significance of this period from our *V*-band data is just barely above the 3σ threshold and needs to be verified.

Solar observations also show evidence for long-term quasi-periodic cycles. Beside the 11 year-long spot cycle, the one with ≈90 years length is also widely known as the Gleissberg-cycle (Gleissberg 1966). Recently, Pipin (1999) introduced a promising numerical model based on a spherical shell dynamo to give an explanation of this secular solar cycle. Compared to the Sun, the data for LQ Hya are still sparse despite that there is now a 21-year long set of broad-band *V* data. However, if scaled to its 16 times faster rotation, the rotational coverage is comparable and we may speculate that the 3.7-year period is reminiscent of the solar 11-year cycle while the 13.8-year trend is reminiscent of the solar Gleissberg cycle.

5.2. Rapid spot evolution

Spot evolution appears to be omnipresent on LQ Hya. The sequence of phase-combined maps in Figs. 3 and 4 and the time-series maps in Fig. 5 manifest spot changes at all our accessable time scales, i.e. within the ≈20 days between the mean epochs of sets "1996/A" and "1996/B" and "2000/A" and "2000/B", within the much shorter time span of ≈6 days between "1996/B" and "1996/C", and even within the ≈1-day resolution of the time-series maps. Most changes appear as waning or waxing of flux rather than as simple spot migrations. Due to the short timescales involved we believe that this kind of events are due to magnetic reconnections on the surface rather than due to the emergence of "fresh" flux tubes from below. Therefore, the equatorial regions of LQ Hya should consist of a mixed polarity field.

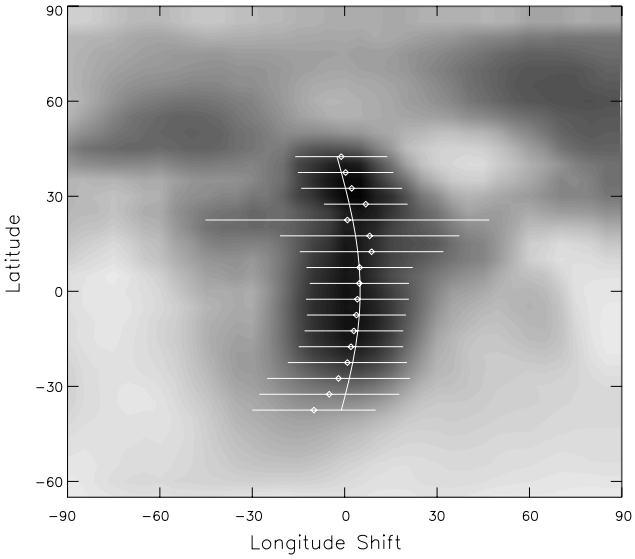

Fig. 6. Average cross-correlation map from the 1996 time series. Black represents perfect correlation, white no correlation. The dots with error bars are the fitted correlation peaks per latitude bin and their rms. The full line is the best-fit solar-type differential rotation law and suggests a shear $\Delta\Omega$ roughly a factor of 3 weaker than on the Sun.

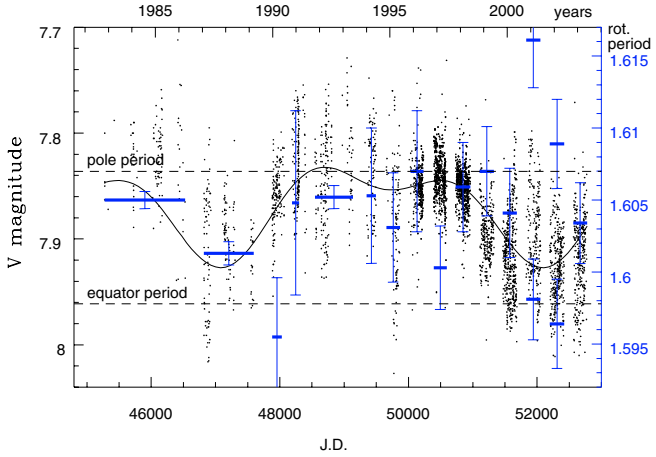

Fig. 7. Seasonal rotation periods of LQ Hya. (When the number of data were insufficient for the period determination, more seasons were used together.) Broken lines mark the period values on the equator and on the pole according to Eq. (2). Most of the derived periods lie within these values confirming their reality. During the seasons of 2001 and 2002 two significant periodicities were found, one of each being slightly longer than the period assigned to the pole.

5.3. Differential surface rotation

We cross correlate consecutive but contiguous maps in the time series from Sect. 4.5, i.e. we compute a cross-correlation-function (ccf) map from image #1 and #9, then one from #2 and #10 and so forth, until the end of the time series. This gives 20 ccf maps. The numerical correlation is done along longitude for all latitudes between −60° and +85° in bins of 5°. Because the time baseline for these ccf maps varied between 10.6 and 17 days, we normalized the longitude shifts to the average time interval of 12.8 days, and then averaged the 20 ccf maps. We then searched for a correlation peak in each latitude strip and fit a Gaussian to it (for a description of the procedure see, e.g., Paper V by Weber & Strassmeier 1998). The longitudinal distribution of the correlation is shown as subsequent latitude strips with grey scale in Fig. 6. For each strip the maximum correlation is represented by the Gaussian peaks (dots) and the corresponding FWHMs (bars). These bars are actually standard deviations from the 20 ccf maps and allow only an estimate of the true error.

The Gaussian peaks were then fitted with a solar-type quadratic differential rotation law of the form

$$\Omega(\theta) = \Omega_{\rm eq} - \Delta\Omega \sin^2\theta, \qquad (2)$$

where θ is the stellar latitude, $\Omega_{\rm eq}$ the equatorial angular velocity, and $\Delta\Omega = \Omega_{\rm eq} - \Omega_{\rm pole}$. The continuous line in Fig. 6 is the best fit with $\Omega_{\rm eq} = 3.932 \pm 0.070$ rad/day, i.e. $P_{\rm eq} = 1.597$ days, and $\Delta\Omega = 0.022 \pm 0.008$ rad/day. The latter translates into a lap time of ≈280 days, i.e. the time the equator needs to lap the pole by one full rotation. The observed photometric period of 1.60066 days (Sect. 3) suggests spots to peak at a latitude of ±33°, in good agreement with the main spot locations in the Doppler maps. The maximum range of spottedness from our images is approximately ±40° above and below the equator (the latter because of symmetry reasons) and thus quite similar to the Sun's. For LQ Hya, we find that $\Delta\Omega/\Omega \approx 0.0057$, as compared to 0.2 as for the Sun, with a shear ($\Delta\Omega$) that is roughly a factor of 3 weaker than on the Sun and at a rotation rate roughly 15 times higher than the Sun's.

We tried to recover the presence of differential rotation from the 21-year long photometric data using the MUFRAN Fourier analysis. The result is shown in Fig. 7, where the seasonal periods are overplotted with the long-term V-light curve. When the number of data points was insufficient for the analysis, more seasons were combined. Figure 7 possibly shows a weak correlation between the seasonal rotational periods and the brightness of the star in the sense that when the star is brighter the rotation is slower. Given our solar-type differential rotation law from Eq. (2), i.e. the equator of LQ Hya rotating faster than the pole, would indicate more high-latitude spots when the star is brighter. The errors of the resulting periods are high, partly due to the limited length of the datasets. Other factors that make the derived seasonal average rotational periods uncertain are the possible spot-latitude changes, new spot appearances at different latitudes and, of course, the differential rotation itself that remains unrecovered in our exercise. However, for the 2001 and 2002 datasets, we find two peaks in the amplitude spectra separated by $0\overset{\rm d}{.}018$ and $0\overset{\rm d}{.}013$ respectively, which may indicate co-existing high-latitude and low-latitude spots but, alternatively, could also be a manifestation of continuous amplitude changes. We will discuss these possibilities in a forthcoming paper.

5.4. A comparison with rising flux-tube models

A stellar-structure model matching LQ Hya is applied to follow the flux tube summits as they rise through the convection zone. This model is only applicable if we presume that the dynamo is located in a shell below the convection zone (see, e.g.,

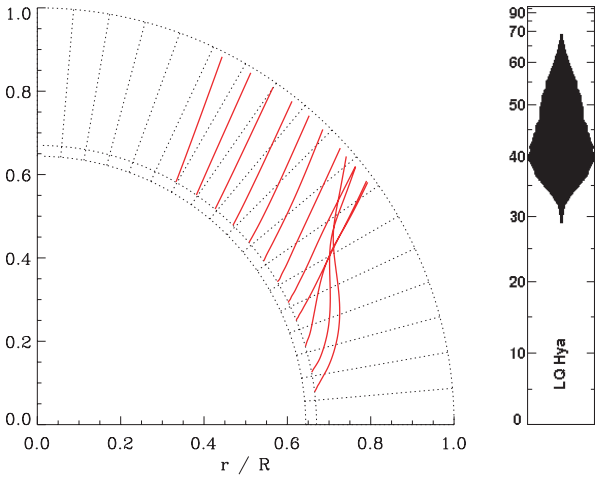

Fig. 8. Flux tube emergence for a 0.8 $M_\odot$ ZAMS star at an age of 100 Myr rotating with $P_{\rm rot}$ = 1.6 d. The cake-pie view shows the meridional projection of trajectories of the emerging flux tubes. The right column represents a smoothed probability of the spot occurrence as a function of latitude.

Stix 2002). We applied a modified version of the MHD code put forward by Schüssler et al. (1996) and others and applied to low-mass stars by Granzer et al. (2000) and, more generally, by Granzer (2002).

The result for LQ Hya is shown in Fig. 8. The upper latitude limit of the spot distribution in our Doppler maps agree with the predicted limit of flux tube emergence, however, the model cannot give account of equatorial spottedness. Due to the fast rotation of LQ Hya flux tubes are always driven away from the equator by the Coriolis force. On the other hand, small scale turbulence and other effects (Choudhuri & D'Silva 1990; D'Silva & Choudhuri 1991) may suppress the Coriolis force and can, at least partially, explain the emergence of flux tubes at lower latitudes. However, the discrepancy between the model and the observations may also imply that the magnetic dynamo is distributed throughout the convective zone rather than that of a boundary-layer type (cf. Deluca et al. 1997). A crude estimate of the global strength of the α and the Ω-effect (see Paternó et al. 2002) for LQ Hya suggests a dominance of the α-effect over the Ω-effect by approximately a factor of 8. Thus, we would rather expect an $\alpha^2\Omega$-dynamo than a solar-type $\alpha\Omega$ dynamo which would (partially) explain the lack of true equatorial spots.

Acknowledgements. K.G.S. is very grateful to the Deutsche Forschungsgemeinschaft for grant STR645/1-3. Zs.K. and K.O. thank for the financial support of the Hungarian OTKA grants T-038013 and T-043504. The authors are also grateful to the German-Hungarian exchange program for grant D-21/2001. Zs.K. would like to express his thanks to Collegium Budapest IAS for providing an outstanding milieu throughout his fellowship.

References

Baraffe, I., Chabrier, G., Allard, F., & Hauschildt, P. H. 1997, A&A, 327, 1054
Berdyugina, S. V., Ilyin, I., & Tuominen, I. 2001, in 11th C.S.S.S.S., ed. R. J. Garcia Lopez, et al., PASPC, 223, CD-ROM
Berdyugina, S. V., Pelt, J., & Tuominen, I. 2002, A&A, 394, 505
Bevington, P. R. 1969, Data Reduction and Error Analysis for the Physical Sciences (New York: McGraw-Hill)
Bidelman, W. P. 1981, AJ, 86, 553
Chabrier, G., & Baraffe, I. 1997, A&A, 327, 1039
Covino, S., Panzera, M. R., Tagliaferri, G., & Pallavicini, R. 2001, A&A, 371, 973
D'Antona, F., & Mazzitelli, I. 1997, in Cool Stars in Clusters and Associations, ed. G. Micela, R. Pallavicini, & S. Sciortino, Mem. S. A. It., 68, 807
Donati, J.-F. 1999, MNRAS, 302, 457
Drake, S. A., Walter, F. M., & Florkowski, D. R. 1990, in 6th C.S.S.S.S., ed. G. Wallerstein, PASPC, 9, 148
Eggen, O. J. 1984, AJ, 89, 1358
ESA 1997, The Hipparcos and Tycho catalog, ESA SP-1200
Fekel, F. C., Bopp, B. W., Africano, J. L., et al. 1986b, AJ, 92, 1150
Fekel, F. C., Moffett, T. J., & Henry, G. W. 1986a, ApJS, 60, 551
Flower, P. J. 1996, ApJ, 469, 355
Gleissberg, W. 1966, J. British Astron. Assoc., 76, 265
Granzer, T. 2002, AN, 323, 395
Granzer, T., Caligari, P., Schüssler, M., & Strassmeier, K. G. 2000, A&A, 355, 1087
Heintz, W. D. 1981, ApJS, 46, 247
Jetsu, L. 1990, ed. K. Muinonen, et al., Proc. Fin. Astr. Soc., 5
Jetsu, L. 1993, A&A, 276, 345
Kitchatinov, L. L., Jardine, M., & Donati, J.-F. 2000, MNRAS, 318, 1171
Kolláth, Z. 1990, MUFRAN, Occasional Technical Notes of Konkoly Observatory, No.1
Kurucz, R. L. 1993, ATLAS-9, CD-ROM No. 13
Montes, D., Saar, S. H., Collier Cameron, A., & Unruh, Y. C. 1999, MNRAS, 305, 45
Oláh, K., & Strassmeier, K. G. 2002, AN, 323, 361
Paternó, L., Belvedere, G., Kuzanyan, K. M., & Lanza, A. F. 2002, MNRAS, 336, 291
Pipin, V. V. 1999, A&A, 346, 295
Piskunov, N. E., & Rice, J. B. 1993, PASP, 105, 1415
Rice, J. B. 2002, AN, 323, 220
Rice, J. B., & Strassmeier, K. G. 1998, A&A, 336, 972 (Paper VII)
Rice, J. B., & Strassmeier, K. G. 2000, A&AS, 147, 151
Rice, J. B., Wehlau, W. H., & Khokhlova, V. L. 1989, A&A, 208, 179
Saar, S. H., Piskunov, N. E., & Tuominen, I. 1994, in 8th C.S.S.S.S., ed. J. P. Caillault, PASPC, 64, 661
Scarfe, C. D., Batten, A. H., & Fletcher, J. M. 1990, Publ. Dominion Astron. Obs. Victoria, 18, 21
Schüssler, M., Caligari, P., Ferriz-Mas, A., Solanki, S. K., & Stix, M. 1996, A&A, 314, 503
Seeds, M. A. 1995, in Robotic telescopes: current capabilities, present developments, and future prospects for automated astronomy, ed. G. W. Henry, & J. A. Eaton, PASPC, 79, 11
Sterzik, M. F., & Schmitt, J. H. M. M. 1997, AJ, 114, 1673
Stix, M. 2002, The Sun, 2nd edition (Berlin: Springer)
Strassmeier, K. G., & Bartus, J. 2000, A&A, 354, 537 (Paper X)
Strassmeier, K. G., Bartus, J., Cutispoto, G., & Rodono, M. 1997, A&AS, 125, 11
Strassmeier, K. G., Boyd, L. J., Epand, D. H., & Granzer, T. 1997, PASP, 109, 697
Strassmeier, K. G., Rice, J. B., Wehlau, W. H., Hill, G. M., & Matthews, J. M. 1993, A&A, 268, 671
Strassmeier, K. G., Serkowitsch, E., & Granzer, T. 1999, A&AS, 140, 29
Weber, M., & Strassmeier, K. G. 1998, A&A, 330, 1029 (Paper V)

Online Material

Table 1. Observing log and radial velocities.

HJD	phase †	v_r (km s^{-1})	σ_{vr} (km s^{-1})	image
2450394.029	0.974	11.8	3.2	1996/A
2450395.025	0.596	5.9	3.1	1996/A
2450396.032	0.225	6.6	3.0	1996/A
2450400.040	0.729	4.6	3.0	1996/A
2450401.035	0.351	6.9	3.1	1996/A
2450405.043	0.855	–	–	1996/A
2450405.980	0.440	6.8	2.9	1996/A
2450406.975	0.062	6.7	2.7	1996/A
2450409.034	0.348	11.7	2.1	1996/B
2450412.000	0.201	9.3	2.5	1996/B
2450412.991	0.820	6.0	2.7	1996/B
2450419.051	0.606	5.9	2.9	1996/B
2450419.995	0.196	8.7	2.6	1996/B
2450420.974	0.808	6.9	2.7	1996/B
2450422.013	0.457	8.2	2.6	1996/C
2450423.007	0.078	8.0	2.7	1996/C
2450425.029	0.341	5.6	3.1	1996/C
2450426.011	0.955	7.9	2.9	1996/C
2450427.014	0.581	7.6	2.9	1996/C
2450429.002	0.823	7.4	2.9	1996/C
2450430.005	0.450	7.8	2.8	1996/C
2450431.009*	0.077	8.3	2.6	–
2450431.875*	0.618	4.2	3.0	–
2450431.955	0.668	6.2	2.8	1996/D
2450433.001	0.322	6.4	2.8	1996/D
2450434.057	0.981	6.5	2.8	1996/D
2450435.017	0.581	7.7	3.0	1996/D
2450436.980	0.807	5.3	3.0	1996/D
2450437.954	0.416	8.4	3.2	1996/D
2450438.946	0.036	8.2	3.0	1996/D
2450440.960	0.294	6.7	2.9	1996/E
2450441.978	0.930	8.8	3.1	1996/E
2450444.966	0.797	6.3[a]	2.3	1996/E
2450446.942	0.031	7.1	2.8	1996/E
2450447.996	0.690	6.2	2.9	1996/E
2450450.047	0.971	5.0	2.9	1996/E
2450450.964	0.544	6.8	3.1	1996/E
2450457.945*	0.905	7.7	2.9	–
2451639.681	0.187	7.1[a]	0.6	2000/A
2451640.647	0.791	7.8[a]	0.6	2000/A
2451641.648	0.416	8.6[a]	0.5	2000/A
2451642.662	0.050	7.4[a]	0.6	2000/A
2451643.744*	0.726	7.6[b]	2.4	–
2451644.677	0.309	8.3[a]	0.6	2000/A
2451660.683	0.308	8.8[a]	0.5	2000/B
2451661.668	0.924	8.7[a]	0.6	2000/B
2451662.652*	0.538	9.5[a]	0.6	–
2451663.654	0.164	7.5[a]	0.5	2000/B
2451664.667	0.797	9.0[a]	0.6	2000/B
2451665.653	0.413	9.8[a]	0.5	2000/B
2451666.661	0.043	8.0[a]	0.5	2000/B
2451667.665	0.670	7.4[a]	0.6	2000/B
2451668.670	0.298	8.1[a]	0.7	2000/B

† for phasing the spectra P_{rot} = 1.600656 days was used
[a] with β Gem (v_r=3.23km s^{-1}) as the velocity standard;
[b] with 16 Vir (v_r=36.48km s^{-1}).
Asterisks indicate spectra with low S/N. The radial-velocity standard star α Ari (v_r = −14.51 km s^{-1} Scarfe et al. 1990) was measured nightly except for a few nights when either β Gem (v_r=3.23km s^{-1}) or 16 Vir (v_r=36.48 km s^{-1}) was observed.

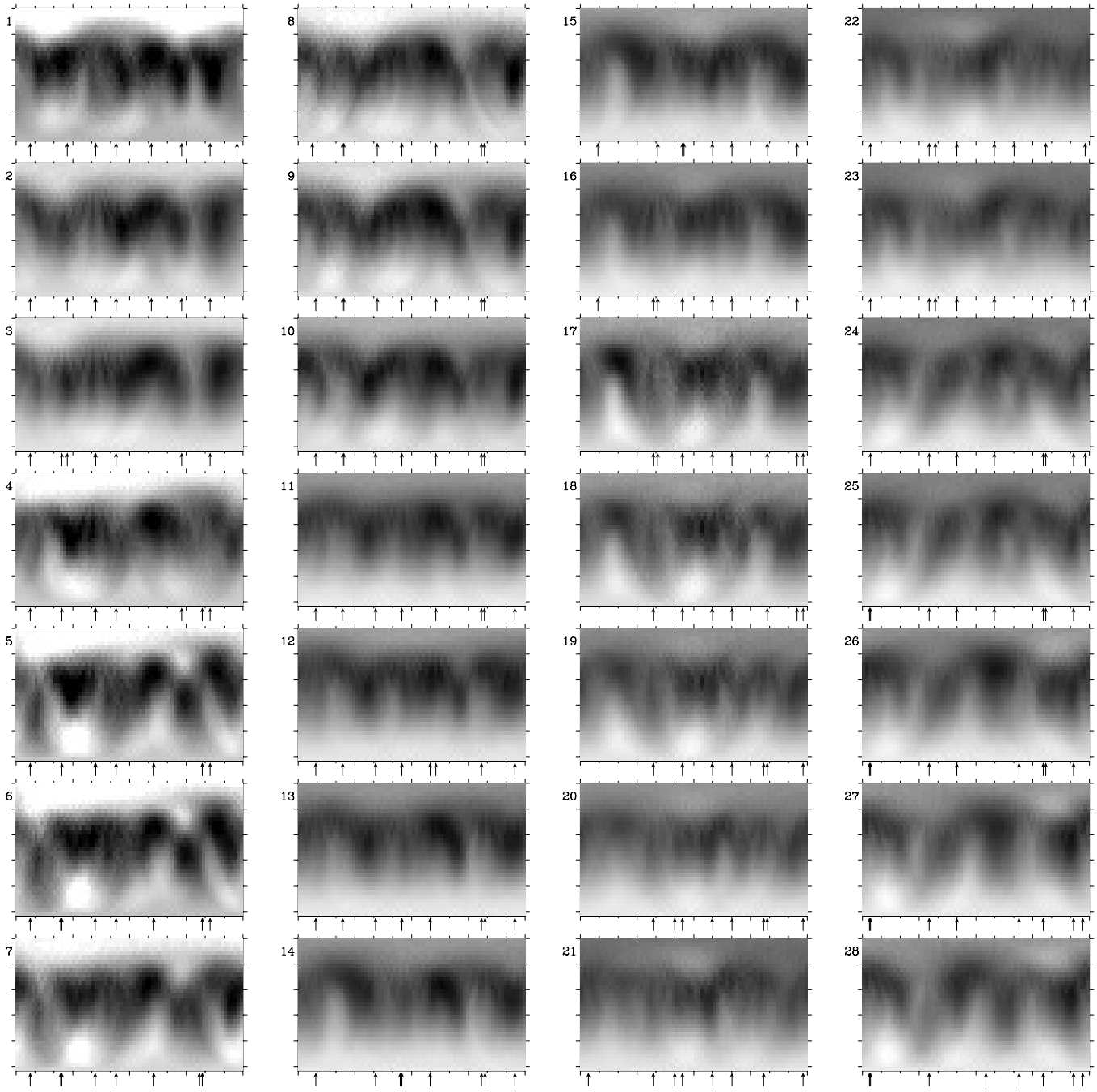

Fig. 5. Time-series Fe I 6430-Å images for Nov.-Dec. 1996. The first map is from the first eight spectra in the series in Table 1, the second map is computed by leaving away the first spectrum but adding the subsequent one, the ninth. This is continued until the last eight spectra in the series are reached and results in altogether 28 maps from a total of 35 stellar rotations. Note that every eighth map is computed from an independent set of profiles. The maps are presented in a pseudo-Mercator projection from latitude −65° to +90°. The phases of the observations are marked by arrows below the maps.